EBioMedicine 63 (2021) 103192

Contents lists available at ScienceDirect

EBioMedicine

journal homepage: www.elsevier.com/locate/ebiom

Research paper

Brain cell-derived exosomes in plasma serve as neurodegeneration biomarkers in male cynomolgus monkeys self-administrating oxycodone

Ashish Kumar[a], Susy Kim[a], Yixin Su[a], Mitu Sharma[a], Pawan Kumar[a], Sangeeta Singh[a], Jingyun Lee[b,c], Cristina M. Furdui[b,c,d], Ravi Singh[a,d], Fang-Chi Hsu[d,e], Jeongchul Kim[f,g], Christopher T. Whitlow[d,e,f,g,h,i], Michael A. Nader[i,j,*], Gagan Deep[a,d,i,k,**]

[a] Department of Cancer Biology, Wake Forest Baptist Medical Center, United States
[b] Department of Internal Medicine, Section on Molecular Medicine, Wake Forest School of Medicine, United States
[c] Proteomics and Metabolomics Shared Resource, Wake Forest Baptist Health, United States
[d] Comprehensive Cancer Center, Wake Forest Baptist Health, United States
[e] Biostatistics and Data Science, Wake Forest Baptist Health, United States
[f] Radiology Informatics and Image Processing Laboratory, Wake Forest School of Medicine, United States
[g] Department of Radiology, Section of Neuroradiology, Wake Forest School of Medicine, United States
[h] Department of Biomedical Engineering, Wake Forest School of Medicine, United States
[i] Center for Research on Substance Use and Addiction, Wake Forest School of Medicine, United States
[j] Department of Physiology and Pharmacology, Wake Forest School of Medicine, Medical Center Boulevard, NRC 546, Winston-Salem, NC 27157, United States
[k] Department of Urology, Wake Forest School of Medicine, Winston-Salem, NC, United States

ARTICLE INFO

Article History:
Received 7 October 2020
Revised 16 November 2020
Accepted 15 December 2020
Available online xxx

Keywords:
Exosomes
Oxycodone
Neuron-derived exosomes
Astrocytes-derived exosomes
Microglia-derived exosomes

ABSTRACT

Background: The United States is currently facing an opioid crisis. Novel tools to better comprehend dynamic molecular changes in the brain associated with the opioid abuse are limited. Recent studies have suggested the usefulness of plasma exosomes in better understanding CNS disorders. However, no study has ever characterized exosomes (small extracellular vesicles of endocytic origin) secreted by brain cells to understand the potential neurodegenerative effects of long-term oxycodone self-administration (SA).
Methods: MRI of Cynomolgus monkeys (Macaca fascicularis) was performed to assess alterations in gray matter volumes with oxycodone SA. We isolated total exosomes (TE) from the plasma of these monkeys; from TE, we pulled-out neuron-derived exosomes (NDE), astrocytes-derived exosomes (ADE), and microglia-derived exosomes (MDE) using surface biomarkers L1CAM (L1 cell adhesion molecule), GLAST (Glutamate aspartate transporter) and TMEM119 (transmembrane protein119), respectively.
Findings: We observed a significantly lower gray matter volume of specific lobes of the brain (frontal and parietal lobes, and right putamen) in monkeys with ~3 years of oxycodone SA compared to controls. Higher expression of neurodegenerative biomarkers (NFL and α-synuclein) correlates well with the change in brain lobe volumes in control and oxycodone SA monkeys. We also identified a strong effect of oxycodone SA on the loading of specific miRNAs and proteins associated with neuro-cognitive disorders. Finally, exosomes subpopulation from oxycodone SA group activated NF-κB activity in THP1- cells.
Interpretation: These results provide evidence for the utility of brain cells-derived exosomes from plasma in better understanding and predicting the pro-inflammatory and neurodegenerative consequence of oxycodone SA.
Funding: NIH

1. Introduction

The United States is currently facing an opioid crisis. In 2017, an estimated 1.7 million individuals suffered from opioid use disorders (OUD) related to prescription opioid pain relievers, and 652,000 suffered from a heroin use disorder. During 2017, there were more than 70,200 overdose deaths in the United States, and 47,600 of those

* Corresponding author at: Department of Physiology and Pharmacology, Wake Forest School of Medicine, Medical Center Boulevard, NRC 546, Winston-Salem, NC 27157, United States.
** Corresponding author at: Department of Cancer Biology, Wake Forest School of Medicine, Medical Center Boulevard, Hanes 5048, Winston-Salem, NC 27157, United States.
E-mail addresses: mnader@wakehealth.edu (M.A. Nader), gdeep@wakehealth.edu (G. Deep).

https://doi.org/10.1016/j.ebiom.2020.103192

Research in Context

Evidence before this study

We searched the PubMed and Google, without restrictions to English language publication using the keywords “Opioid AND exosomes”, “Oxycodone AND exosomes”, “Oxycodone and neurodegeneration” and “Oxycodone and miRNAs”. We unbiasedly included all the relevant studies showing the molecular and neurodegenerative effect of opioid/oxycodone. Many studies also demonstrated the usefulness of plasma-derived exosomes to predict the patho-psychological changes in the brain. Furthermore, studies have shown the adverse effect of opioids on the central nervous system in experimental mouse/rat models and human subjects. Though, in most of the studies, the neurotoxicity related to opioids/oxycodone was studied on isolated brain/cells or used complicated brain imaging techniques to understand the effects of oxycodone. We conducted the study with the aim to explore the usefulness of specific brain cells-derived exosomes from plasma to interpret the effect of oxycodone SA on neurodegeneration.

Added value of this study

Herein, we performed a prospective study correlating the brain cells-derived exosomes, isolated from the plasma of control and oxycodone SA monkeys, with alteration in gray matter volume of specific lobes of the brain. We observed the presence of neurodegeneration biomarkers, including proteins and miRNAs in exosomes isolated from plasma of monkeys exposed to oxycodone for ~3years. This is the first study to provide evidences that neurodegenerative effects caused by long-term oxycodone exposure in non-human primates could be accessed by studying cargos loaded in the brain cells-derived exosome subpopulations isolated from the plasma.

Implications of all the available evidence

Our findings propose the potential use of exosomes as a source of biomarkers to predict the possible neurodegenerative and pro-inflammatory effect following oxycodone abuse. The present study offers a novel exosomes based less invasive approach to better understand the molecular and biological effects of oxycodone and other drugs of abuse. The study provides evidences that these plasma-based nano-tools could be used as biosignatures of opioid addiction, as well as to assess the benefits of various therapeutic interventions.

overdose deaths involved opioids. Opioids bind to receptors in the brain and spinal cord, disrupting pain signals but also activating brain reward systems in the ventral striatum, elevating dopamine and opioid peptides, as well as stress systems in the extended amygdala [1, 2]. Oxycodone, a semi-synthetic opioid, was first synthesized in 1916, ironically in an attempt to provide a potent opioid analgesic devoid of the dependence and abuse liability issues plaguing heroin. Over the past two decades, oxycodone has become the opioid with the largest increase in distribution by volume and number of prescriptions [3].

The effects of opioids abuse on the central nervous system (CNS) have been well investigated in preclinical and clinical studies [4-15]. In animal models, heroin-addicted rats demonstrated neuronal cell death in the cerebellum [14]. Similarly, rats treated with morphine expressed cognitive deficit [10] and apoptosis in neuronal cells [15]. Chronic oxycodone exposure in rats caused axonal degeneration, loss of myelin basic protein, accumulation of several neurodegeneration biomarkers (Aβ and its precursor protein APP, phosphorylated tau, and α-synuclein), and activation of pro-apoptotic machinery [11]. Several studies have also reported that opioids adversely affect glial cells, including a decrease in myelin insulation provided by oligodendrocytes, activation of inflammatory astrocytes, and microglia leading to neurodegeneration [11, 12, 16]. Oxycodone SA in mice significantly altered the synaptic plasticity gene expression in the hippocampus [17]. In humans, leukoencephalopathy, axon demyelination, and lesions in white matter were documented mostly with heroin abusers [4, 5] but also in methadone, morphine, and oxycodone over-dosed patients [6–8]. In 2010, a study investigating brain structures in prescription opioid-dependent patients demonstrated structural and functional changes in brain regions responsible for impulse control, reward, and motivation [9]. Autopsy studies have reported neuropathological changes in young drug abusers similar to those seen with Alzheimer's disease (AD) [12, 13]. However, compared to animal studies where the adverse effects of opioids are evident, similar direct correlations between opioid use and neurocognitive effects in humans have been harder to establish due to various confounding factors such as chronic pain (severity and duration), comorbidities, depressive symptoms, physical activity and smoking status [18]. This suggests the need for blood-based molecular tools to comprehend dynamic molecular changes in the brain associated with the opioid abuse.

Exosomes are small extracellular vesicles (~30–150 nm) that are released by all cell types. Their biogenesis and release into the extracellular environment involves the formation and fusion of clathrin-coated vesicles with the endosome, inward budding of the membrane of endosomes, cargo loading leading to the formation of multivesicular endosomes (MVEs), and MVE fusion with the plasma membrane. Exosome contents are protected from degradation while in circulation, making these vesicles an efficient means for local and distant intercellular communication [19]. Exosomes are present in all biofluids and are loaded with cargo, including RNAs, proteins, lipids, and metabolites that could relate to the cell of origin and the physiologic and metabolic state [20–24]. For these reasons, exosomes are being extensively studied for the diagnosis and prognosis of diseases such as AD, Parkinson's, multiple sclerosis, and cancer [19, 20, 24–30]. Importantly, brain cell-derived exosomes are present in the circulation and are being examined as potential mediators of AD-related pathological changes [31–33]. Levels of Aβ and P-tau in neuronal-derived exosomes predicted AD development before any clinical symptoms [29, 34]. These studies suggest that brain cells-derived exosomes could cross the blood-brain barrier (given their nano size) and get into peripheral circulation, probably through transcellular (through brain microvascular endothelial cells) or paracellular (junctions between brain microvascular endothelial cells) pathways [35]. Importantly, the microRNAs associated with circulating exosomes successfully diagnosed multiple sclerosis and accurately predicted disease subtype [36]. Similarly, exosomes have also been used in predicting treatment outcomes in cancer patients [37, 38], kidney transplantation [39], myocardial recovery after MitraClip repair [40], and hepatitis C patients [41].

Exosomes isolation from several biofluids have been employed to define molecular biomarkers associated with drug abuse and associated side effects [42–53]. Several studies have analyzed proteins and miRNAs cargo loaded in exosomes to envisage the consequential adverse effects of different drugs, including alcohol [46–48, 54]. In animal studies, Li et al. identified ten key miRNAs in serum exosomes associated with the development of addiction to methamphetamine and ketamine in rats [45]. Hu et al. reported that astrocytes treated with morphine and HIV Tat secreted exosomes containing miR-29b can be taken up by the neurons resulting in neuronal death [43]. This study also demonstrated that exosomal miR-29b was associated with morphine's *in vivo* effects. Toyama et al. identified several circulating miRNAs that were differentially expressed following oxycodone

treatment in males and could serve as surrogates of μ-opioid receptor signaling [55]. Dominy et al. identified unique proteins in the saliva of HIV+ heroin addicts associated with neurocognitive disorder, and most of the identified proteins were associated with exosomes [44]. Shahjin et al. identified distinct brain-derived extracellular vesicles (EVs) miRNA signatures associated with in-utero and postnatal oxycodone exposure [52]. These studies suggest the utility of exosomes to identify molecular biomarkers associated with drug addiction.

However, most of the studies related to drug abuse were conducted either on small animals (i.e. mice, rats, etc.) or conducted after short-term exposure to the drug. In these scenarios, it is difficult to predict the effect of these drugs on human's especially following long-term exposure. Here, we used non-physically dependent male cynomolgus monkeys with ~3-years of oxycodone histories to assess the long-term effects of oxycodone SA on the volume of various brain regions. We further characterized the brain cells (neuron, astrocytes, and microglia) derived exosomes in plasma from both control and oxycodone SA monkeys for various neurodegeneration biomarkers (NFL, α-synuclein, and Aβ1−42), proteome, and specific set of miRNAs. We also assessed the effect of NDE from control and oxycodone SA groups on subcellular localization of glucocorticoid receptor (GR) in astrocytes. Finally, we compared the pro-inflammatory effect of brain cells-derived exosomes from control and the oxycodone group in terms of their effect on NF-κB activity in monocytes. Results from the present study suggest an exosome-based novel molecular approach to understand the potential neurodegenerative effects of oxycodone.

2. Methods

2.1. Subjects

Six, individually housed, adult male (10−13 years old) cynomolgus macaques (*Macaca fascicularis*) served as subjects. Three monkeys were experimentally naïve at the start of this study, while three monkeys had been self-administering oxycodone for ~3 years. Monkeys in the oxycodone SA group were surgically prepared with an indwelling intravenous catheter as described before [56]; oxycodone (0.001−0.17 mg/kg/injection) was available under a fixed-ratio (FR) and progressive-ratio (PR) schedules of reinforcement, Mondays thru Fridays; FR sessions ended after 30 injections or 60-min, while PR sessions ended after a limited hold of 30-min, which was typically < 2 h or up to 15 injections/session. Under these conditions, animals did not develop physical dependence on oxycodone. Under both schedules, the dose-response curves were represented as an inverted-U shaped functions of dose for each monkey. Typically, doses were kept constant for at least five consecutive sessions. Total oxycodone intakes varied from 50 to 170 mg/kg. During this study, control monkeys were trained under a concurrent schedule of reinforcement in which they chose between 1- and 3-g banana-flavored pellets during daily 1-h operant sessions. These animals served as controls for the effects of operant condition on brain cells-derived exosomes. Monkeys lived in a temperature- and humidity-controlled room maintained on a 14-h light/10-h dark cycle (lights on between 6:00 AM and 8:00 PM) in stainless-steel cages with ad-libitum access to water. Monkeys were fed sufficient standard laboratory chow (Purina LabDiet 5045, St Louis, Missouri, USA) to maintain healthy body weights slightly below free-feeding weights and enriched daily with fresh fruits or vegetables. In awake monkeys, while seated in primate restraint chair, blood (2−3 ml) was collected via venous femoral vein in Covidien Monoject 3 mL drawtubes containing EDTA (K3) 0.06 ml 7.5% solution. Following blood collection, the tubes were immediately placed on ice and within 5−10 min tubes were spun for 15 min, 3000 RPM at 4 °C. Plasma was then collected and frozen in 0.5 ml aliquots and stored at minus 30 °C.

2.2. Ethics

Animal housing, handling, and experimental protocols were performed in accordance with the 2011 National Research Council Guidelines for the Care and Use of Mammals in Neuroscience and Behavioral Research and were approved by the Animal Care and Use Committee of Wake Forest University (A18−126). Environmental enrichment was provided as outlined in the Animal Care and Use Committee of Wake Forest University Non-Human Primate Environmental Enrichment Plan, including chew toys, mirrors, music, and foraging feeders.

2.3. Total exosomes (TE) and brain cells-derived exosomes isolation and characterization

TE were isolated from the 500 μl of plasma of control monkeys (abbreviated as $TE^{Control}$) and oxycodone SA monkeys (abbreviated as $TE^{Oxycodone}$) using the ExoQuick (System Biosciences, Palo Alto California, USA) precipitation method as described by us previously [22, 57]. For the isolation of cell type-specific exosomes, 400 μl of streptavidin magnetic beads (ThermoFisher Scientific, Waltham, MA, USA) were washed twice with 400 μl of isolation buffer (0.1% BSA in PBS) and re-suspended in 250 μl of the same buffer. For antibody labeling, magnetic beads were incubated with 1 μg of biotin-labeled antibodies against cell type-specific surface proteins expressed on the exosomes i.e. L1CAM/CD171-Biotin (for NDE) (Cat. No. 13-1919-82, ThermoFisher Scientific), GLAST (Cat. No. ACSA-1-Biotin, Miltenyi Biotec, Auburn, California, USA) (for ADE) and TMEM119 (Cat. No. 853302, BioLegend, San Diego, California, USA) (for MDE), at room temperature for 1 h with continuous mixing. TMEM119 antibody was labeled with biotin using FluoReporter Mini-biotin-XX protein labeling kit (Invitrogen, Carlsbad, California, USA) as recommended by the manufacturer. Antibody labeled magnetic beads were incubated overnight (~16 h) with total exosomes (500 μg) at 4 °C with continuous mixing. Beads were then magnetized and supernatant (negative exosome population) was removed. Beads were further washed four times with 400 μl of isolation buffer before final re-suspension in 200 μl of the same buffer. 25 μl of beads (with exosomes attached) were aliquoted in a separate tube for flow cytometry analysis to validate the specific exosomes population.

2.4. Nanoparticle tracking analysis (NTA)

Quantification of the hydrodynamic diameter distribution and concentration of exosomes was performed using the Nanosight NS300 (Malvern Instruments, UK) equipped with a violet laser (405 nm) and running software version NTA3.2. The instrument was primed using phosphate-buffered saline, pH 7.4 (PBS), and the temperature was maintained at 25 °C. Accurate nanoparticle tracking was verified using 50 nm and 200 nm polystyrene nanoparticle standards (Malvern Instruments) prior to examination of the samples. Five measurements (30 s each) were obtained for each sample.

2.5. Western blotting

Exosome markers proteins were identified by Western blotting. 20 μg of TE from both control and oxycodone SA monkeys were pooled (n = 3/group), denatured directly in 2x sample loading buffer and subjected to sodium dodecyl sulfate-polyacrylamide gel electrophoresis on 8−12% Tris-glycine gel (as required based upon the protein molecular weight). The separated proteins were transferred on to nitrocellulose membrane followed by blocking with 5% non-fat milk powder (w/v) in Tris-buffered saline (10 mM Tris−HCl, pH 7.5, 100 mM NaCl, 0.1% Tween 20) for 1 h at room temperature. Membranes were probed for the desired protein using specific primary antibodies: CD9 (Cat. No. ab92726), CD31 (Cat. No. ab28364), Alix

(Cat no. ab88388) (all three from Abcam, Cambridge, Massachusetts, USA), HSP70 (Cat. No. 4872S), Calnexin (Cat no. 2679s) (both from Cell Signaling Technology, Beverly, Massachusetts, USA). This was followed by the appropriate peroxidase-conjugated secondary antibody and visualized by the ECL detection system. The autoradiograms/bands were scanned using Adobe Photoshop 6.0 (Adobe Systems, San Jose, CA).

2.6. Flow cytometry

To validate the purity of cell-type-specific exosomes isolated using magnetic beads, flow cytometry analysis was performed. Briefly, magnetic beads bound exosomes were labeled with respective fluorophore tagged antibodies at room temperature for 1 h with continuous mixing. L1CAM antibody was labeled with PE, GLAST antibody with APC (both from BioLegend), and TMEM119 antibody with Cy5. TMEM119 antibody was labeled with Cy5 using the Cy5 conjugation Kit (Abcam, Cambridge, Massachusetts, USA). Following incubation, beads were washed three times with isolation buffer. The supernatant was removed by magnetizing the beads. Finally, beads were re-suspended in 200 μl of PBS and analyzed by the BD Accuri C6 flow cytometer (BD Biosciences, San Joes, California, USA). Bead-bound exosomes tagged with these antibodies were captured with FL-2 and FL-4 channels. Data was analyzed using BD Accuri C6 software. The specificity was tested by adding a non-specific antibody to a specific bead-bound exosome population for flow analysis e.g. GLAST-APC antibody was added to the NDE isolated using L1CAM labeled beads or L1CAM-PE was added to ADE isolated using GLAST-labelled beads and analyzed by flow cytometry.

2.7. miRNA expression analysis

For miRNA isolation from the exosomes subpopulation, magnetic beads (following exosomes isolation) were re-suspended in 500 μl of Trizol reagent directly and incubated at RT for 10 min with intermittent vortexing. Following incubation, beads were magnetized and removed, 100 μl of chloroform was added to the tube and mixed. Tubes were centrifuged for 15 min at 14,000$\times$ g at 4°C. The top clear layer was recovered, and after the addition of 2−3 vol of 100% ethanol, incubated at −80 °C for 2 hrs. RNA was further washed and eluted (in 22 μl of RNase free water) using and following the recommendation of RNAeasy mini kit (Qiagen, Maryland, USA). cDNA was synthesized with 25 ng of total RNA using Taqman advanced miRNA cDNA synthesis kit (Applied Biosystems, Foster City, California, USA) with 14 cycles of enrichment. All the real-time PCR analyses were performed with "Taqman advanced miRNA assay" (Applied Biosystems) using 1 μl of synthesized cDNA. To normalize the miRNA expression data Normfinder and RefFinder software were used to identify the most stable miRNAs that can be used as reference control to calculate $\Delta\Delta$Ct values.

2.8. Enzyme−linked immunosorbent assay (ELISA)

Following isolation of cell type-specific exosomes isolation using magnetic beads, exosomes were lysed by adding RIPA buffer directly to the beads. Magnetic beads were then magnetized and removed, and exosomes lysate was collected and quantified using the BCA method. For total exosomes, RIPA buffer was added to the exosomes and incubated on ice for 30 min with intermittent vortexing. 5 μg of exosomes lysate was used to identify the neurodegeneration markers using ELISA Kits i.e. α-synuclein (Invitrogen, Carlsbad, California, USA), Aβ1−42 (R&D Systems, Minneapolis, Minnesota, USA), NFL (Abbexa, Houston, Texas, USA) and p-Tau (pS199), p-Tau (pT231) (both from Invitrogen, Carlsbad, California, USA) as per the manufacturers' recommendation. The samples were analyzed in duplicates from independent experiments. The absolute concentration of the marker proteins were calculated from the respective standards and data are represented in pg/ml or ng/ml.

2.9. Immuno-cytochemistry

Normal human astrocytes cells were purchased from Lonza (Lonza, California, USA) and maintained in AGM astrocyte growth medium (Lonza, USA) as per the vendor's recommendations. To assess the effect of NDE treatment on GR, astrocytes were seeded on poly-lysine coated coverslip in 6 well plate at a density of 10,000 cells/cm^2. Cells were treated with 5×10^8 NDE^{Control} or NDE^{Oxycodone} and incubated for 24 h. Following incubation, cells were fixed with chilled acetone for 10 min at −20 °C. Coverslips with cells were washed three times with PBST (PBS with 0.1% tween-20) and incubated with antibody against GR (Cat. no.12041S, Cell Signaling Technology, Massachusetts, USA) at 1:200 dilution, overnight at 4 °C. Cells were further washed three times with PBST and incubated with secondary antibody tagged with Alexa fluor 647 (Cell Signaling Technology, USA) at 1:200 dilution for 1 h at RT. Finally, cells were washed three times with PBST and mounted on a glass slide with antifade mounting with DAPI (Vector Laboratories, California, USA). Slides were imaged with Olympus FV1200 spectral laser scanning confocal microscope with 40X oil objective lens.

2.10. NF-κB activation assay

For the analysis of the inflammatory response of NDE, ADE, and MDE, the NF-κB activation assay was performed on THP-1 Lucia NF-κB monocyte cells (purchased from InvivoGen, San Diego, California, USA). The cell line was not validated but all the experiments were performed at early cell passages only. The THP-1 Lucia NF-κB cell line contains a stable NF-κB inducible Lucia reporter construct which is secreted to the growth medium. THP-1 Lucia cells were maintained in RPMI 1640 media supplemented with 2 mM L-glutamine, 25 mM HEPES, 10% heat-inactivated fetal bovine serum and Pen-Strep (100 U/ml-100 μg/ml). Cells were maintained by passaging every 3−4 days by inoculating 0.5−1 $\times$ 10^6 cells to fresh medium. For NF-κB activation assay, cells were seeded at 50,000 cells per well in a 96 well plate and co-cultured with 10 μg of (NDE^{Control}, NDE^{Oxycodone}, ADE^{Control}, ADE^{Oxycodone}, MDE^{Control}, and MDE^{Oxycodone}) for 16−18 h. After incubation, 20 μl of media was taken in 96 well black-walled clear bottom imaging plate (BD Falcon, Tewksbury, Massachusetts, USA). The activity of secreted luciferase was detected using QUANTi-Luc Gold, luminescence detection reagent (InvivoGen, San Diego, California, USA) as per the manufacturers' recommendation.

2.11. Proteomics analysis

LC-MS grade Water (Cat. Num. W6−4), acetonitrile (Cat. Num. A955−4), LC-MS grade formic acid (Cat. Num. A117−50), and MS grade trypsin protease (Cat. Num. 90059) were purchased from ThermoFisher Scientific (Waltham, MA, USA).

Exosomes suspended in PBS were lysed by the addition of an equal volume of 2x radioimmunoprecipitation (RIPA) buffer containing protease inhibitor cocktail. The protein extract (10 μg) was subjected to reducing alkylation with 10 mM dithiothreitol and 30 mM iodoacetamide followed by protein precipitation with cold acetone. The protein pellet was then suspended in 50 mM ammonium bicarbonate and proteolytically digested with 0.4 μg of trypsin at 37 °C overnight. Peptides were purified using a C18 spin column and prepared in 5% (v/v) ACN containing 1% (v/v) formic acid for LC-MS/MS analysis.

Peptides were analyzed on an LC-MS/MS system consisting of an Orbitrap Velos Pro-Mass Spectrometer (Thermo Scientific, Waltham, MA) and a Dionex Ultimate-3000 nano-UPLC system (Thermo

Scientific, Waltham, MA) equipped with an Acclaim PepMap 100 (C18, 5 μm, 100 Å, 100 μm x 2 cm) trap column and an Acclaim PepMap RSLC (C18, 2 μm, 100 Å, 75 μm x 50 cm) analytical column. MS spectra were acquired by the top ten data-dependent scans with a dynamic exclusion option of 30 s enabled.

Spectra were searched using Sequest HT within the Proteome Discoverer v2.2 (Thermo Scientific, Waltham, MA) and UniProt human protein FASTA database (20,258 annotated entries, Feb 2018). Search parameters were as follows: FT-trap instrument, parent mass error tolerance of 10 ppm, fragment mass error tolerance of 0.6 Da (monoisotopic), variable modifications of 16 Da (oxidation) on methionine, and fixed modification of 57 Da (carbamidomethylation) on cysteine. Signal-to-noise ratio (STN) was determined following similar approaches as published [58]. Proteomics data was analyzed using Ingenuity Pathway Analysis (IPA) (QIAGEN Inc., https://www.qiagenbioinformatics.com/products/ingenuitypathway-analysis) as described earlier [59].

2.12. MRI

Monkeys were sedated with 15 mg/kg ketamine HCl (IM) and transported to the MRI Center where they were imaged under isoflurane (3% induction, 1.5% maintenance) anesthesia. Structural brain imaging data were collected using a 3 Tesla Siemens MAGNETOM Skyra (Siemens Healthcare, Erlangen, Germany) with a pediatric 32-channel head coil. Anatomical images were acquired using a T1-weighted MPRAGE sequence: TR = 2700 ms, TE = 3.32 ms, inversion time = 880, FOV = 128 × 128 mm, 192 slices of 0.5 mm thickness, resolution = 0.5 mm isotropic. The Radiology Informatics and Image Processing Laboratory (RIIPL) conducted structural image processing and analysis based on their NHP imaging pipeline [60, 61]. Briefly, bias field correction, denoising, and intensity normalization were performed using the N4BiasFieldCorrection function of Advanced Normalization Tools (ANTs, Penn Image Computing and Science Laboratory, University of Pennsylvania, PA). Next, an initial whole-head study-specific template (SST) was created for the purpose of skull stripping using ANTs (antsMultivariateTemplateConstruction.sh) after rigid-body alignment to a UNC Primate Atlas [61]. Following skull-stripping, the UNC Template brain was registered to the SST brain and transformed the UNC parcellation map, brain mask, and segmentation priors to the SST using deformable registration. The full parcellation consisted of separate definitions for the left and right hemisphere for the subcortical, frontal, prefrontal, cingulate, parietal, occipital, auditory, visual, and limbic temporal lobes, as well as the brainstem and cerebellum. Cortical labels in the parcellation map included gray matter, white matter, and cerebrospinal fluid (CSF); and subcortical structures, including the hippocampus, amygdala, caudate, and putamen.

2.13. Statistical analysis

All the experiments for ELISA and miRNAs expression analyses were performed in triplicates and repeated 2–3 times. Values were plotted as average using GraphPad Prism 7.0 software (La Jolla, CA). Statistical significance was calculated by unpaired t-tests. Significance was considered at $p < 0.05$. Correlations between gray matter brain volumes and neurodegenerative markers were calculated using Spearman's rank correlation coefficient estimates in SAS 9.4 software (SAS Inc., Cary, North Carolina, USA).

2.14. Role of funding source

The funders had no role in study design, data collection, data analysis, interpretation or writing of the report.

3. Results

3.1. Effect of oxycodone SA on the gray matter volume of various brain regions

We first characterized the effect of oxycodone SA on gray matter volume of various brain regions of interest namely, both right and left, occipital, temporal auditory, subcortical, frontal, cerebellum, insula, cingulate, parietal, prefrontal, temporal visual, temporal limbic, pons and medulla, hippocampus, amygdala, caudate, and putamen. As shown in Fig. 1, gray matter volume was significantly lower in the oxycodone SA group compared to controls in the frontal lobe (left and right), putamen (right), and parietal lobe (left and right).

3.2. Characterization of exosomes

Total exosomes (TE) were isolated from the plasma of control ($n = 3$) and oxycodone SA monkeys ($n = 3$) by ExoQuick precipitation method, and exosome populations were abbreviated as $TE^{Control}$ and $TE^{Oxycodone}$, respectively. The size and concentration of $TE^{Control}$ and $TE^{Oxycodone}$ was analyzed by NTA. As shown in Fig. 2A, the mean size of $TE^{Oxycodone}$ (133.2 nm) was significantly larger compared to $TE^{Control}$ (102.6 nm), however, no significant difference in the exosome concentration (number per ml) was observed between the two groups (Fig. 2B). The concentration and size distribution for each exosome sample ($TE^{Control}$ and $TE^{Oxycodone}$) is presented in Supplementary Fig. S1. $TE^{Control}$ and $TE^{Oxycodone}$ were also characterized for exosomal biomarker proteins CD9, CD31, Alix, and HSP70 (Fig. 2D). We did not observe any expression of endoplasmic reticulum protein Calnexin, which is usually not present in exosomes.

Next, unique surface protein biomarkers were employed to isolate three different exosomes subpopulations from $TE^{Control}$ and $TE^{Oxycodone}$: L1CAM to isolate neuron-derived exosomes (NDE), GLAST to isolate astrocyte-derived exosomes (ADE), and TMEM119 to isolate microglia-derived exosome (MDE). Each exosome population was characterized by flow cytometry (FACS) (Fig. 2D). For flow analysis, exosomes were labeled with specific fluorophore tagged antibodies and analyzed by BD Accuri C6 flow cytometer. Black peaks in Fig. 2D represent the fluorescence from beads only, and green and purple peaks represent the shift in fluorescence because of the binding of fluorophore antibody to the exosomes from control and oxycodone SA animals, respectively. The purity of exosome populations was confirmed by labeling NDE with GLAST antibody and ADE with the L1CAM antibody, in both cases no detectable cross-contamination between the exosomes subpopulations was observed (Supplementary Figure S2).

3.3. Effect of oxycodone SA on neurodegeneration biomarkers in exosomes

Next, by ELISA method, we analyzed the TE, NDE, ADE, and MDE from control and oxycodone SA monkeys for NFL, α-synuclein, and Aβ1–42 expression, established biomarkers for neurodegeneration. As shown in Fig. 3, $TE^{Control}$ and $TE^{Oxycodone}$, as well as $MDE^{control}$ and $MDE^{oxycodone}$, did not show significant differences in the levels of any neurodegeneration marker. However, a significantly higher NFL level was observed in $NDE^{Oxycodone}$ (Fig. 3A). Similarly, significantly higher level of α-synuclein was observed in $NDE^{Oxycodone}$ and $ADE^{Oxycodone}$ (Fig. 3B). Interestingly, relatively low expression of Aβ1–42 was observed in both $NDE^{Oxycodone}$ and $ADE^{Oxycodone}$ compared to $NDE^{Control}$ and $ADE^{Control}$, respectively (Fig. 3C). We also analyzed the expression of p-Tau (pS199) and p-Tau (pT231), but no detectable expression was observed in any of the exosomes population (data not shown). Finally, we performed a correlation analysis with neurodegeneration markers and the brain gray matter volumes for both control and oxycodone SA monkeys. We did not observe any significant correlation between TE_Aβ1–42 and TE_NFL with any of the

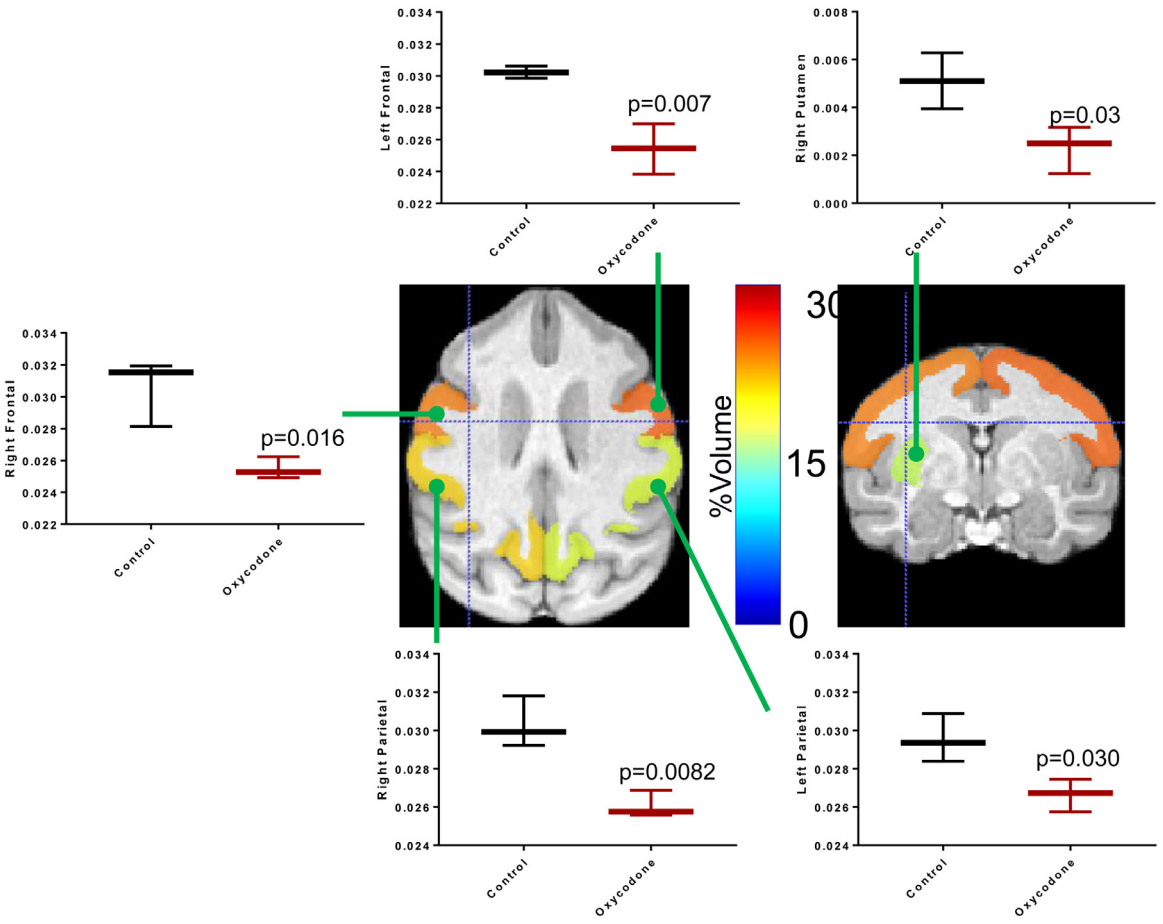

Fig. 1. Effect of oxycodone self-administration (SA) on gray matter volume. Axial and coronal slices through brain demonstrate percent difference in gray matter volume among oxycodone SA monkeys ($n = 3$) compared to controls ($n = 3$) according to the color bar (% difference compared to control computed from quantitative gray matter volume provided on the graphs), with red indicating relatively large and blue indicating relatively small% difference in gray matter volume. Gray matter volume was significantly ($p<0.05$) lower among oxycodone SA monkeys compared to controls in the frontal lobes (Left Frontal $p = 0.007$, t ratio=5.104, degree of freedom (df)=4; Right Frontal $p = 0.016$, t ratio=4, df=4), parietal lobes (Right Parietal $p = 0.0082$, t ratio= 4.87, df=4; Left Parietal, $p = 0.030$, t ratio= 3.29, df=4), and putamen ($p = 0.03$, t ratio=3.194, df=4) .

analyzed brain lobe gray matter volumes. TE_α-synuclein showed a negative correlation with right frontal and left parietal gray matter volume. Interestingly, NDE_ Aβ1−42 levels showed a positive correlation with left amygdala gray matter volume. Further, we observed a negative correlation between NDE_NFL levels and frontal lobe (right and left), left parietal lobe, and left putamen gray matter volume (Table 1). A similar strong negative correlation was observed between the levels of NDE_α-synuclein and right frontal and left parietal. ADE_ Aβ1−42 showed a positive correlation with the left putamen, amygdala (right and left). ADE_α-synuclein levels also showed statistically significant negative correlations with the right frontal lobe, left frontal lobe, and left parietal lobe gray matter volume. MDE_Aβ1−42 levels showed a positive correlation with left cingulate and left parietal (Table 1).

3.4. Effect of oxycodone on a panel of miRNAs associated with cognition, depression, anxiety, and neurodegeneration

Next, the effect of oxycodone SA was examined on the expression of nine miRNAs (Let7a-5p, miR16−5p, miR-18−5p, miR107, miR-125−5p, miR-144−3p, miR-210−3p, miR-339−3p, and miR-361−5p), which are known to be associated with neurocognitive dysfunctions and neurodegeneration or show differential expression following oxycodone treatment [55, 62-66]. miR-125−5p, as confirmed by RefFinder and Normfinder software, was found to be the most stable miRNA expressed in all three exosome subpopulations and used for normalization (Supplementary Fig. S3). As shown in Fig. 4, the expression of different miRNAs varied depending upon the exosome type. For example, miR16−5p, miR-18−5p, and miR-339−3p were significantly lower and miR-361−5p, and miR-144−3p were significantly higher in $NDE^{Oxycodone}$ compared to $NDE^{Control}$ (Fig. 4A). Similarly, miR16−5p was significantly lower while miR-107, miR-339−3p, and miR-144−3p were significantly higher in $ADE^{Oxycodone}$ compared to $ADE^{Control}$ (Fig. 4B). Also, miR16−5p, and miR-361−5p were significantly lower; and Let7a-5p, miR-107, miR-339−3p, and miR-144−3p were significantly higher in $MDE^{Oxycodone}$ compared to $MDE^{Control}$ (Fig. 4C). However, we could not detect the expression of miR-210 in any of the exosomes populations.

3.5. Exosomes are loaded with unique proteins

Next, we characterized the proteins loaded in exosomes. Mass spectrometry analyses identified in total 160 proteins in NDE, 161 in ADE, 237 in MDE, and 175 proteins loaded in TE. $NDE^{Oxycodone}$ showed a higher expression of 33 proteins compared to $NDE^{Control}$ (STN $\geq$0.3) and decreased loading of 75 proteins (STN ≤ -0.3). $ADE^{Oxycodone}$ showed a higher expression of 80 proteins compared to $ADE^{Control}$ (STN $\geq$0.3) and decreased loading of 17 proteins (STN ≤ -0.3). $MDE^{Oxycodone}$ showed a higher expression of 46 proteins compared to $NDE^{Control}$ (STN $\geq$0.3) and decreased loading of 96 proteins (STN ≤ -0.3). $TE^{Oxycodone}$ showed a higher expression of 23 proteins compared to $TE^{Control}$ (STN $\geq$0.3) and decreased loading of 92 proteins (STN ≤ -0.3).

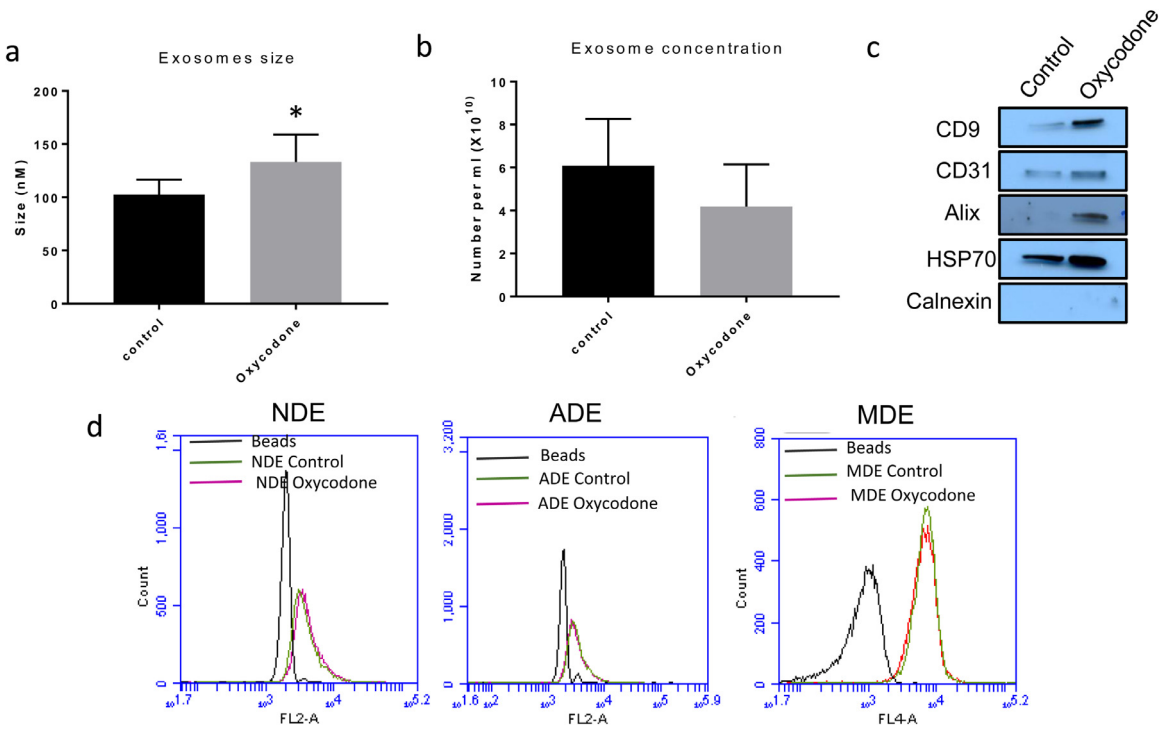

Fig. 2. Characterization of exosomes. (a-b) Total exosomes were analyzed for size distribution and concentration by nanoparticle tracking analysis (NTA). Exosomes samples were analyzed in three independent experiments in both control and oxycodone SA monkeys ($n = 3$/group). Exosome size and concentration are presented as mean±SEM of three independent experiments $^{*}p<0.01$ (t ratio=3.12, degree of freedom (df)=16). (c) Characterization of exosomal biomarker proteins by immunoblotting. (d) NDE, ADE, and MDE were isolated from total exosomes using biotin-tagged specific antibodies and streptavidin-tagged magnetic beads as described in the methods. Exosomes were labeled with specific fluorophore tagged antibodies and images acquired on BD Accuri C6 flow cytometer. Representative FACS images are shown..

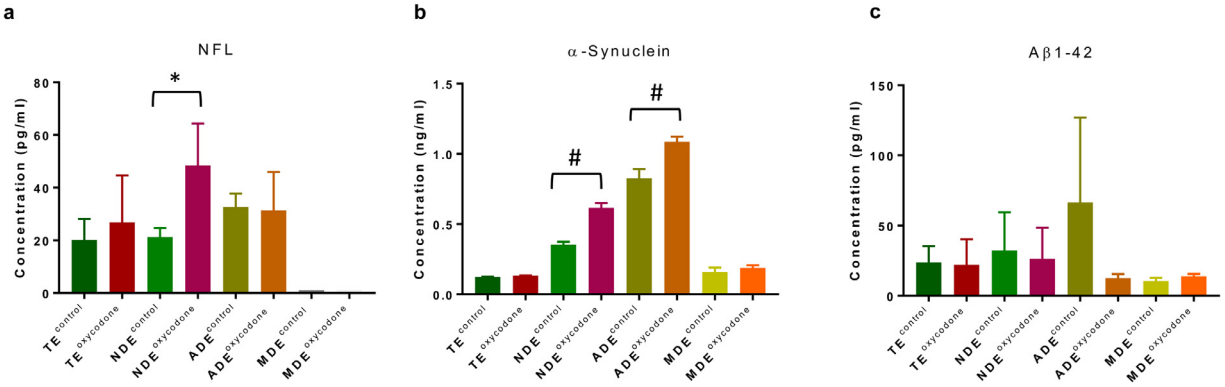

Fig. 3. Effect of oxycodone SA on neurodegeneration biomarkers in exosomes. Protein expression of neurodegeneration biomarkers (NFL, α-synuclein and Aβ1−42) was analyzed in total exosomes, NDE, ADE, and MDE from control and oxycodone SA monkeys by ELISA. Each experiment was performed in triplicate. Concentrations of each marker was calculated by generating a standard curve. The data are presented as mean±SD. $^{*}p<0.05$; $\#p<0.01$ $^{*}p<0.05$ (NFL: t ratio= 2.868, df=4); $\#p<0.01$ (α-synuclein, NDE: t ratio= 11.69; ADE: t ratio= 5.992, df=4).

Next, higher abundance proteins (STN ≥0.3) in the oxycodone SA group were analyzed by IPA, and their association with various diseases and disorders are presented in Fig. 5A. Higher expression of proteins in TE, NDE, ADE, and MDE in response to oxycodone SA are summarized in Supplementary Table S1A and S1B. NDE^{Oxycodone} showed association with neurological and psychological disorders, while ADE^{Oxycodone}, MDE^{Oxycodone}, and TE^{Oxycodone} were associated with immunological and inflammatory diseases (Fig. 5A). Further, IPA analyses of higher proteins (STN ≥0.3) in NDE^{Oxycodone} identified the following top-upstream regulators: MAPT (p-value=9.24E-17); APP (p-value=6.31E-14); and PSEN1 (p-value=5.69E-13) (Fig. 5B), which are widely known to be involved in neurological disorders [67-70]. The top-network of proteins altered in NDE^{Oxycodone} is shown in Fig. 5C. Interestingly, several of these molecules (CREB, ERK1/2, TGFβ, and S100B, etc.) are widely known for their role in addiction-related molecular circuitries [71−73]. Similarly, IPA analyses of proteins with higher abundance in ADE^{Oxycodone} (STN ≥0.3) showed enrichment in proteins associated with the following major pathways: glucocorticoid receptor signaling; gluconeogenesis; glycolysis; complement system; and TCA cycle (Fig. 5D). Major canonical pathways associated with higher abundant proteins in NDE^{Oxycodone}, MDE^{Oxycodone}, and TE^{Oxycodone} are shown in Supplementary Fig. S4.

3.6. NDE^{oxycodone} induces glucocorticoid receptor (GR) translocation to the nucleus and systemic pro-inflammatory response

Based upon the strong association of ADE^{Oxycodone} protein cargo with GR signaling (Fig. 5D), we next assessed the effects of NDE on GR nuclear translocation in astrocytes. Astrocyte cells were treated with 5×10^8 NDE isolated from both control and oxycodone SA

Table 1
Correlation between gray matter volume of specific lobes of the brain and various exosomal markers ($n = 6$). p-values are shown in *italics* to represent the significant correlation (highlighted in bold) for each brain lobe with neurodegenerative markers.

Spearman Correlation Coefficients, $N = 6$ Prob > |r| under H0: Rho=0	TE_Aβ1−42	NDE_Aβ1−42	ADE_Aβ1−42	MDE_Aβ1−42	TE_NFL	NDE_NFL	ADE_NFL	MDE_NFL	TE_α-synuclein	NDE_α-synuclein	ADE_α-synuclein	MDE_α-synuclein
R_Subcortical	0.31429	0.42857	0.71429	−0.37143	−0.08571	−0.63775	0.6	−0.65465	−0.48571	−0.48571	−0.6	0.25714
p-value	*0.5441*	*0.3965*	*0.1108*	*0.4685*	*0.8717*	*0.1731*	*0.208*	*0.1583*	*0.3287*	*0.3287*	*0.208*	*0.6228*
R_Frontal	0.31429	0.48571	0.6	−0.82857	−0.2	−0.92763	0.37143	−0.65465	−0.82857	−0.82857	−0.94286	0.31429
p-value	*0.5441*	*0.3287*	*0.208*	***0.0416***	*0.704*	***0.0077***	*0.4685*	*0.1583*	***0.0416***	*0.0416*	***0.0048***	*0.5441*
R_Parietal	−0.37143	0.37143	0.08571	−0.6	0.14286	−0.72471	−0.31429	−0.13093	−0.71429	−0.71429	−0.77143	0.48571
p-value	*0.4685*	*0.4685*	*0.8717*	*0.208*	*0.7872*	*0.1032*	*0.5441*	*0.8047*	*0.1108*	*0.1108*	*0.0724*	*0.3287*
L_Frontal	0.37143	0.42857	0.65714	−0.65714	−0.37143	−0.92763	0.54286	−0.65465	−0.77143	−0.77143	−0.82857	0.42857
p-value	*0.4685*	*0.3965*	*0.1562*	*0.1562*	*0.4685*	***0.0077***	*0.2657*	*0.1583*	*0.0724*	*0.0724*	***0.0416***	*0.3965*
L_Cingulate	0.65714	0.48571	0.65714	−0.82857	−0.31429	−0.72471	0.48571	−0.65465	−0.6	−0.6	−0.77143	0.02857
p-value	*0.1562*	*0.3287*	*0.1562*	***0.0416***	*0.5441*	*0.1032*	*0.3287*	*0.1583*	*0.208*	*0.208*	*0.0724*	*0.9572*
L_Parietal	0.02857	0.37143	0.25714	−0.88571	−0.14286	−0.89865	−0.02857	−0.39279	−0.88571	−0.88571	−0.94286	0.37143
p-value	*0.9572*	*0.4685*	*0.6228*	***0.0188***	*0.7872*	***0.0149***	*0.9572*	*0.4411*	***0.0188***	***0.0188***	***0.0048***	*0.4685*
L_Putamen	0.65714	0.54286	0.82857	−0.6	−0.54286	−0.86966	0.71429	−0.65465	−0.6	−0.6	−0.71429	0.37143
p-value	*0.1562*	*0.2657*	***0.0416***	*0.208*	*0.2657*	***0.0244***	*0.1108*	*0.1583*	*0.208*	*0.208*	*0.1108*	*0.4685*
R_Putamen	−0.02857	0.42857	0.48571	−0.37143	−0.08571	−0.7537	0.25714	−0.39279	−0.6	−0.6	−0.65714	0.54286
p-value	*0.9572*	*0.3965*	*0.3287*	*0.4685*	*0.8717*	*0.0835*	*0.6228*	*0.4411*	*0.208*	*0.208*	*0.1562*	*0.2657*
R_Amygdala	0.71429	0.65714	0.88571	−0.6	−0.31429	−0.69573	0.65714	−0.65465	−0.42857	−0.42857	−0.65714	0.14286
p-value	*0.1108*	*0.1562*	***0.0188***	*0.208*	*0.5441*	*0.1248*	*0.1562*	*0.1583*	*0.3965*	*0.3965*	*0.1562*	*0.7872*
L_Amygdala	0.71429	0.94286	0.88571	−0.31429	−0.6	−0.63775	0.42857	−0.13093	−0.08571	−0.08571	−0.37143	0.48571
p-value	*0.1108*	*0.0048*	***0.0188***	*0.5441*	*0.208*	*0.1731*	*0.3965*	*0.8047*	*0.8717*	*0.8717*	*0.4685*	*0.3287*

*p-values were not corrected for multiple comparisons.

monkeys, and GR subcellular localization was analyzed by confocal microscopy. As shown in representative photomicrographs in Fig. 6A (also see Supplementary Fig. S5), astrocytes treated with $NDE^{oxycodone}$ showed robust nuclear translocation of GR, suggesting its activation. The quantification of fluorescent images showed an approximately two-fold higher translocation of GR to the nucleus following $NDE^{oxycodone}$ treatment (Fig. 6B).

Since we consistently observed inflammatory disease associated with overabundant proteins in exosomes from the oxycodone SA group, next, we assessed the effect of exosomes treatment on the NF-κB activity in monocytes, as a molecular surrogate of inflammation. As shown in Fig. 6C, treatment with $NDE^{Oxycodone}$, $ADE^{Oxycodone}$, and $MDE^{Oxycodone}$ strongly induced the NF-κB activity in THP1 cells compared to $NDE^{Control}$, $ADE^{Control}$, and $MDE^{Control}$, respectively.

4. Discussion

In the present study, we assessed the usefulness of plasma exosomes to serve as nano-tools to better understand the molecular alterations and biological effects of long-term oxycodone abuse. The main findings are: (a) distinct brain cells-derived exosome populations (NDE, ADE, and MDE) could be isolated from plasma and offer valuable information about neurodegeneration biomarkers compared to TE; (b) exosomal cargo (protein and miRNA) could provide molecular mechanistic information about systemic and CNS-related adverse effects of oxycodone SA; (c) brain cells-derived exosomes could mediate systemic pro-inflammatory effects of oxycodone SA; and (d) oxycodone SA negatively affects gray matter volume of specific lobes of the brain which correlates with the neurodegenerative biomarkers (e.g., NFL) detected in NDE and ADE (Fig. 6D).

Several prior studies have suggested the potential neurodegenerative effects of opioid abuse [9, 12, 13]. Opiate-mediated depression of respiration could potentially lead to hypoxic brain injury and vascular changes, including the breakdown of the blood-brain barrier, associated with significant structural alterations, neuroinflammation, and predisposition to neurodegenerative diseases [9, 12, 13]. Ramage et al. characterized the brain of opiate abusers and concluded that hyper-phosphorylated tau and β-amyloid precursor protein (β-APP) deposition was increased in the brains of young drug abusers, possibly due to hypoxic-ischemic injury, microglial associated cytokine release, and drug-associated neurotoxicity [13]. However, we could not detect the expression of master hypoximir miR-210 in any of the exosomes subpopulation (data not shown). In a subsequent study, the same group concluded that drug users show early Alzheimer's disease-related brain pathology, which could be the basis for cognitive impairment [12], although these studies were performed in the postmortem brain. In this regard, results from the present study are significant as neurodegeneration biomarkers (NFL, α-synuclein, and Aβ1−42) were detected in brain cells-derived exosomes (NDE, ADE, and MDE) from the plasma which significantly correlated with volume changes in several brain lobes (Fig. 3 and Table 1). Also, differential cargos (proteins and miRNAs) loaded in the exosomes isolated from oxycodone SA monkeys provide essential insight into the neuropathological/pro-inflammatory consequential effects of oxycodone. Opioids, including oxycodone, have been correlated with alterations in brain structures and neurodegeneration, resulting in dementia or cognitive decline [11, 18], as opioid receptors are distributed throughout the brain, including the cognitive regions of the frontal and parietal lobe. In the present study, we have identified higher expression of NFL in $NDE^{oxycodone}$ and α-synuclein in $NDE^{oxycodone}$ and $ADE^{oxycodone}$, which negatively correlates with frontal and parietal lobes' volume and suggests the usefulness of these exosomes in predicting neurodegeneration and cognitive impairment following long-term oxycodone SA. Further, this observation is corroborated with the previous study by Rohrer et al. that showed a correlation of serum concentration of NFL with frontal lobe atrophy rate [74]. These

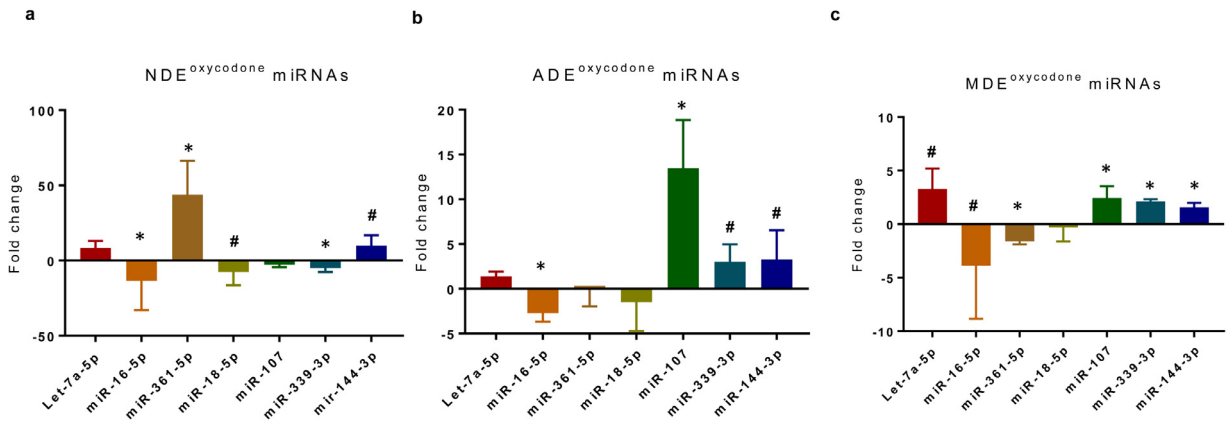

Fig. 4. Effect of oxycodone SA on a panel of miRNAs in exosomes. Expression profiling miRNAs in NDE, ADE, and MDE was performed by real-time PCR. Exosomal miRNA expression profiling of oxycodone treated monkeys was calculated by normalizing expression with control monkeys (ΔCt). miR-125−5p was used as a reference to calculate the fold change (ΔΔCt method). Experiments were run in triplicates. * $p<p.001$,df=4, #$p<0.05$, df=4.

observations offer a novel opportunity to use plasma exosomes as biomarkers to assess the adverse neurocognitive and neurodegenerative effects of opioids and other drugs on CNS as well as to follow the outcome of any intervention.

Exosomes are secreted by all cell types and play a key role in local and distant intercellular communication via their unique cargo (e.g., proteins, miRNA, and metabolites, etc.). In the present study, we characterized the proteins loaded in exosomes by mass spectrometry. The detailed analyses of exosomal cargo proteins identified several interesting proteins involved in neurological disorders, inflammation, and stress signaling. The over-abundant proteins loaded in NDE^{Oxycodone} suggested an association with neurological disease and several upstream regulators (MAPT, APP, and PSEN1) commonly associated with AD. Mass spectrometry analysis of NDE^{Oxycodone} also revealed the enrichment of HSPA8/HSC70, which along with HSP90 is required for GR signaling activation [75]. We also confirmed the potential of NDE^{Oxycodone} in eliciting GR nuclear translocation in astrocytes, which suggests a possibility that NDE^{oxycodone} could induce a stress response in neighboring astrocytes. Similarly, over-abundant proteins, including HSPA5 loaded in ADE^{Oxycodone} showed a strong correlation with GR signaling, which is associated with stress response in astrocytes [76]. We also observed that the over-abundant proteins loaded in TE^{Oxycodone} were associated with inflammation and immunological disorders and diseases. Moreover, the NDE^{Oxycodone} and ADE^{oxycodone} showed higher expression of α-synuclein, which has previously been correlated with higher systemic immune activation in patients of Parkinson's disease [77, 78]. In mass spectrometry analysis, we observed loading of several proteins in exosome, which are reported to have a pro-inflammatory response, i.e., glial fibrillary acidic protein [79], ficolin-2 [80], thrombospondin-1 [81], Fibulin-1 [82], S100A8 [83] and gelsolin [84]. Interestingly, in line with this differential loading of pro-inflammatory proteins in NDE^{Oxycodone}, ADE^{Oxycodone}, and MDE^{Oxycodone}, we observed that these exosomes strongly induced the NF-κB activity in THP-1 cells, suggesting a strong systemic pro-inflammatory effects of exosomes secreted by neurons, astrocytes, and microglia in response to oxycodone. However, the direct effect of

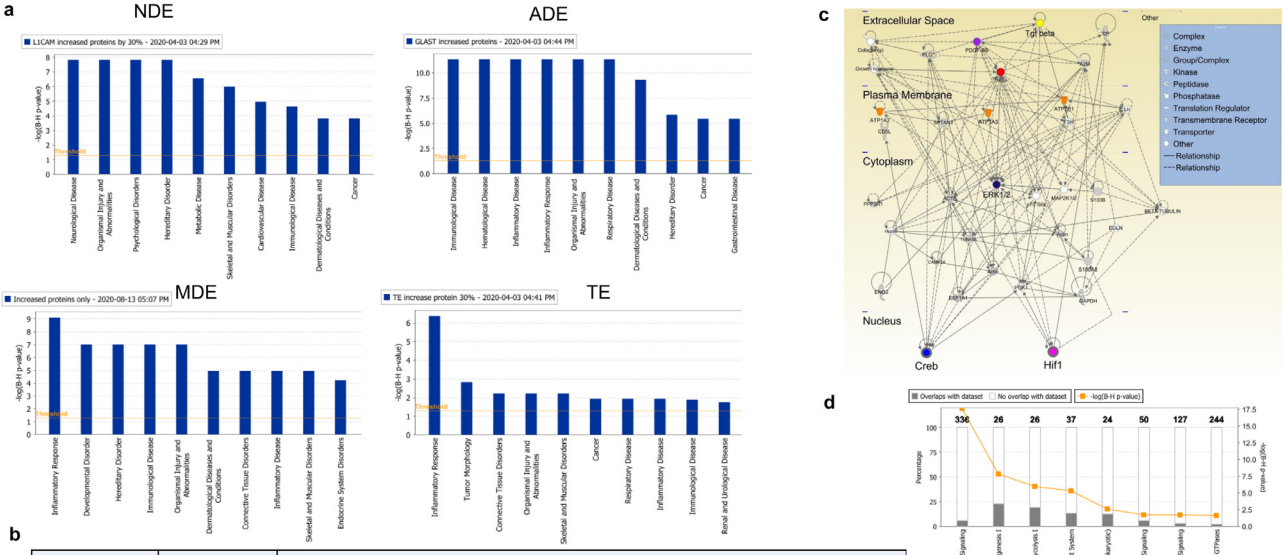

b

Upstream Regulator	p-Value of overlap	Target Molecules in Dataset
MAPT	1.30E-17	ACTB, ALB, ATP1A2, ATP1A3, ATP5F1A, CAMK2A, ENO2, GAPDH, PGK1, PPP3R1, S100B, SPTAN1, TUBA1A
APP	3.76E-14	ACTB, ALB, ATP1A2, ATP1A3, ATP5F1A, CD5L, CP, ENO2, GAPDH, PGK1, S100B, SPTAN1, TUBA1A
PSEN1	6.01E-14	ACTB, ALB, ATP1A2, ATP1A3, ATP5F1A, ENO2, GAPDH, PGK1, S100B, SPTAN1, TUBA1A

Fig. 5. Exosomal proteome analyses by IPA. (a) Disease and disorders associated with overabundant proteins in NDE^{Oxycodone}, ADE^{Oxycodone}, MDE^{Oxycodone}, and TE^{Oxycodone}. (b-c) Upstream regulators and top-network associated with overabundant proteins in NDE^{Oxycodone}. (d) Canonical pathway associated with overabundant proteins in ADE^{Oxycodone}.

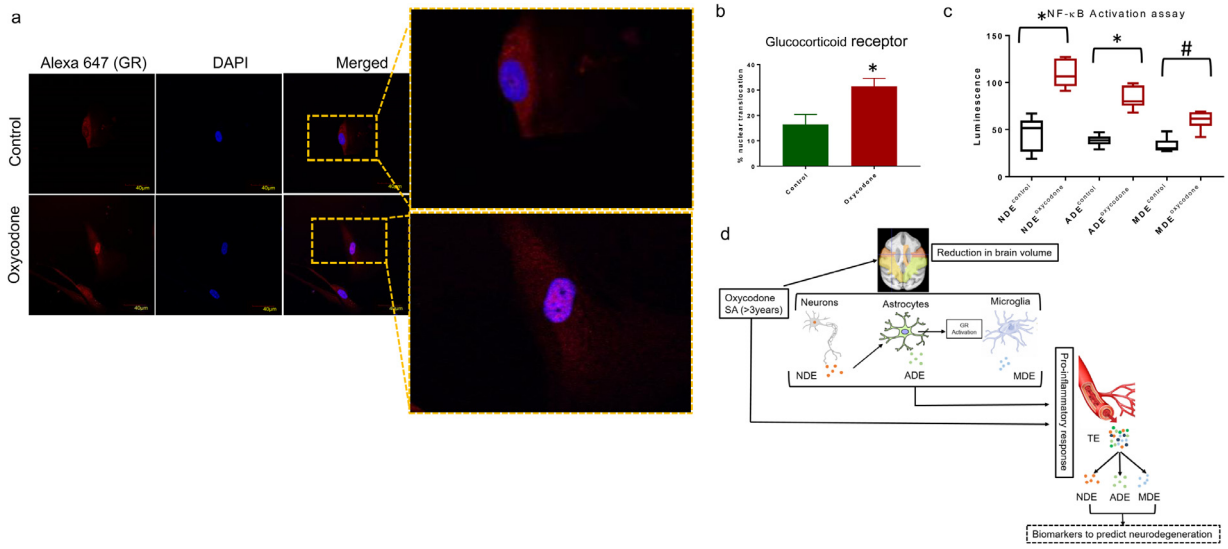

Fig. 6. Effect of exosomes from oxycodone SA monkeys on GR sub-cellular localization in astrocytes and NF-κB activity in THP1 monocytes. (a) Normal human astrocytes were treated with NDE from both control and oxycodone SA monkeys and incubated for 24 h. Cells were fixed and labeled with GR antibody followed by Alexa fluor 647 tagged secondary antibody. Cells were imaged with Olympus FV1200 spectral laser scanning confocal microscope with 40x objective lens. Insets show a magnified portion of a part of the image. (b) 8–10 images of all the treated groups were captured, and the percentage nuclear translocation of GR was calculated by Image J software. $^{*}p<0.01$(represented as mean ± SD) t ratio= 5.169, df= 4. (c) THP-1 cells were treated with NDE, ADE, or MDE (10 ug/well) isolated from the plasma of control and oxycodone SA monkeys. NF-κB activity was measured after 18 h. Experiments were performed in duplicate for 3 samples in each group. $^{*}p<0.0001$; $\#p<0.0005$ (represented as mean ± SD) (NDE t ratio= 6.512, ADE t ratio= 8.393, MDE t ratio= 5.268, df= 10. (d) Schematic representation showing the oxycodone adverse effects, and usefulness of plasma exosomes in predicting the neurodegenerative and pro-inflammatory response of oxycodone SA.

oxycodone on astrocytes, microglia, or monocytes could not be ruled out, and also, exosomes and other secretions of each cell type could affect the other cells.

Besides proteins, exosomes are also loaded with miRNAs, and we observed significant modulatory effects of oxycodone on the expression of specific exosomal miRNAs associated with neurodegeneration, cognition, anxiety, and depression. We consistently observed higher expression of Let-7a-5p miRNA, and higher expression of this miRNA has previously been reported following opioid exposure [55]. Let-7 miRNA was reported to be involved in pathways of apoptosis, autophagy, cell cycle regulation, glycolysis/gluconeogenesis, MAPK signaling pathway, and PI3K-Akt signaling pathway. Knockdown of Let-7 miRNA was shown to reduce the expression of α-synuclein expression [85]. Moreover, higher expression of Let-7 has frequently been observed in C. elegans model of Parkinson's disease [85, 86]. Lehmann et al. showed elevated levels of Let-7 levels in the CSF of AD patients and also reported that Let-7 is capable of activating intrinsic cell death pathways in cultured neurons via Toll-like receptor 7 [62]. Such stimulation could result in increased production of inflammatory cytokines by microglia that corroborate with our observation that $MDE^{Oxycodone}$ induces NF-κB activity in monocytes. miR-16–5p, another miRNA that showed consistent expression, was found to be significantly lower in $NDE^{Oxycodone}$, $ADE^{Oxycodone}$, and $MDE^{Oxycodone}$. Decreased expression of miR-16–5p was reported in SH-SY5Y cells after the treatment of amyloid β [87]. Also, expression of miR-16–5p was detected in the serum of AD patients, and its expression was reduced with the increase in the Braak stage of AD [88]. In line with our data, expression of miR-16–5p was also found to be downregulated following 24 h exposure of hydromorphone and oxycodone in healthy male subjects [55]. Similarly, the expression of miR-107 was reported to be reduced in Aβ-treated cells, and its overexpression reversed Aβ-induced injury [89]. Furthermore, the expression of miR-107 was down-regulated in dementia patients [90] and has been suggested as a potential blood-based biomarker for disease risk and progression of AD [91]. These reports support our observation that lower expression of miR-107 in $NDE^{Oxycodone}$ could be associated with neurodegeneration. These results suggest the usefulness of exosomal miRNAs to serve as biosignatures of opioid abuse as well as associated adverse effects such as neurodegeneration, anxiety, and depression.

There are few limitations of this study, including a low number of replicates ($n = 3$ for both control and oxycodone), even though the current data suggest the potential of exosomes to distinguish between control and oxycodone SA monkeys. Although unlikely, another potential limitation of the study was that the control monkeys did not have an indwelling intravenous catheter, to control for the possibility that some of the group differences were due to inflammatory responses due to the ~ 3 years of catheter implantation. Also, it is difficult to determine whether the exosomes isolated based on specific surface marker proteins (L1CAM, GLAST, and TMEM119) are from central and/or peripheral regions; these exosomes can still present a potential tool to predict the consequential neurodegenerative and pro-inflammatory effect of oxycodone SA. In addition, it is difficult to establish the direct functional impact of the circulating exosomes derived from the brain cells on other organs and also among the neuronal network given the complexity of cellular populations involved in their release and uptake. Moreover, with the current technical limitations it is difficult to predict the target cell types which possibly could uptake the brain cells-derived exosomes, however the exosomes derived from studied brain cells (NDE, ADE and MDE) were found to be loaded with proteins and miRNAs that can have implications in inflammatory responses and neurodegeneration, so it can be concluded that these exosomes can evoke systemic inflammatory response and propagate the neurodegenerative signaling. However, we agree that a detailed study with a larger cohort is needed to establish exosomes as potential blood-based biomarkers to study the effect of oxycodone SA. Furthermore, we need to study expression of these neurodegeneration biomarkers in cerebrospinal fluid (CSF) and/or molecular brain imaging, wherever possible, (e.g. PET imaging by PiB tracer for Aβ).

In summary, the present study offers a novel approach to better understand the molecular and biological effects of oxycodone and other drugs of abuse in a less invasive manner. The exosomes derived from brain cells following oxycodone SA can also serve the surrogate biomarkers to predict the patho-physiological status of the host brain cells. These plasma-based nano-tools could be used to identify

molecular biosignature of opioid addiction, as well as to assess the efficacy of various therapeutic interventions.

Declaration of Competing Interest

The authors have declared that no conflict of interest exists.

Data sharing

Materials used in this study are commercially available. Study-specific primary cell or any other material can be provided upon availability and written request to the corresponding authors. There is no restriction on the availability of any data.

Acknowledgment

We acknowledge the outstanding technical assistance of Michael Coller, Jillian Odom, Chrystal Bragg, Stephanie Rideout Susan Nader, and Richard Barcus.

Funding

This work was supported by R01DA049267 (to GD and MAN) and R01DA017763 (MAN), and R01MH116675 (CTW). Authors also acknowledge WFBCCC Cellular Imaging Shared Resource, Cell Engineering shared Resources, and the Proteomics and Metabolomics Shared Resource supported by NCI (P30CA012197, PI: Dr. Boris Pasche), as well as the Translational Imaging Program of the Clinical and Translational Science Institute (UL1TR001420).

Supplementary materials

Supplementary material associated with this article can be found, in the online version, at doi:10.1016/j.ebiom.2020.103192.

References

[1] Uhl GR, Koob GF, Cable J. The neurobiology of addiction. Ann N Y Acad Sci 2019;1451(1):5–28.
[2] Koob GF. Neurobiology of opioid addiction: opponent process, hyperkatifeia, and negative reinforcement. Biol. Psychiatry 2020;87(1):44–53.
[3] Remillard D, Kaye AD, McAnally H. Oxycodone's unparalleled addictive potential: is it time for a moratorium? Curr. Pain Headache Rep. 2019;23(2):15.
[4] Offiah C, Hall E. Heroin-induced leukoencephalopathy: characterization using MRI, diffusion-weighted imaging, and MR spectroscopy. Clin Radiol 2008;63(2):146–52.
[5] Li W, Li Q, Zhu J, Qin Y, Zheng Y, Chang H, et al. White matter impairment in chronic heroin dependence: a quantitative DTI study. Brain Res 2013;1531:58–64.
[6] Zanin A, Masiero S, Severino MS, Calderone M, Da Dalt L, Laverda AM. A delayed methadone encephalopathy: clinical and neuroradiological findings. J Child Neurol 2010;25(6):748–51.
[7] Eran A, Barak M. Posterior reversible encephalopathy syndrome after combined general and spinal anesthesia with intrathecal morphine. Anesth Analg 2009;108(2):609–12.
[8] Morales Odia Y, Jinka M, Ziai WC. Severe leukoencephalopathy following acute oxycodone intoxication. Neurocrit Care 2010;13(1):93–7.
[9] Upadhyay J, Maleki N, Potter J, Elman I, Rudrauf D, Knudsen J, et al. Alterations in brain structure and functional connectivity in prescription opioid-dependent patients. Brain 2010;133(Pt 7):2098–114.
[10] Spain JW, Newsom GC. Chronic opioids impair acquisition of both radial maze and Y-maze choice escape. Psychopharmacology (Berl) 1991;105(1):101–6.
[11] Fan R, Schrott LM, Arnold T, Snelling S, Rao M, Graham D, et al. Chronic oxycodone induces axonal degeneration in rat brain. BMC Neurosci 2018;19(1):15.
[12] Anthony IC, Norrby KE, Dingwall T, Carnie FW, Millar T, Arango JC, et al. Predisposition to accelerated Alzheimer-related changes in the brains of human immunodeficiency virus negative opiate abusers. Brain 2010;133(Pt 12):3685–98.
[13] Ramage SN, Anthony IC, Carnie FW, Busuttil A, Robertson R, Bell JE. Hyperphosphorylated tau and amyloid precursor protein deposition is increased in the brains of young drug abusers. Neuropathol Appl Neurobiol 2005;31(4):439–48.
[14] Pu H, Wang X, Zhang J, Ma C, Su Y, Li X, et al. Cerebellar neuronal apoptosis in heroin-addicted rats and its molecular mechanism. Int J Clin Exp Pathol 2015;8(7):8260–7.
[15] Mao J, Sung B, Ji RR, Lim G. Neuronal apoptosis associated with morphine tolerance: evidence for an opioid-induced neurotoxic mechanism. J Neurosci 2002;22(17):7650–61.
[16] Rodriguez M. A function of myelin is to protect axons from subsequent injury: implications for deficits in multiple sclerosis. Brain 2003;126(Pt 4):751–2.
[17] Zhang Y, Brownstein AJ, Buonora M, Niikura K, Ho A, Correa da Rosa J, et al. Self administration of oxycodone alters synaptic plasticity gene expression in the hippocampus differentially in male adolescent and adult mice. Neuroscience 2015;285:34–46.
[18] Dublin S, Walker RL, Gray SL, Hubbard RA, Anderson ML, Yu O, et al. Prescription Opioids and Risk of Dementia or Cognitive Decline: a Prospective Cohort Study. J Am Geriatr Soc 2015;63(8):1519–26.
[19] Kumar A, Deep G. Exosomes in hypoxia-induced remodeling of the tumor microenvironment. Cancer Lett 2020;488:1–8.
[20] Eissa S, Matboli M, Aboushahba R, Bekhet MM, Soliman Y. Urinary exosomal microRNA panel unravels novel biomarkers for diagnosis of type 2 diabetic kidney disease. J Diabetes Complications 2016;30(8):1585–92.
[21] Schlaepfer IR, Nambiar DK, Ramteke A, Kumar R, Dhar D, Agarwal C, et al. Hypoxia induces triglycerides accumulation in prostate cancer cells and extracellular vesicles supporting growth and invasiveness following reoxygenation. Oncotarget 2015;6(26):22836–56.
[22] Ramteke A, Ting H, Agarwal C, Mateen S, Somasagara R, Hussain A, et al. Exosomes secreted under hypoxia enhance invasiveness and stemness of prostate cancer cells by targeting adherens junction molecules. Mol Carcinog 2015;54(7):554–65.
[23] de Jong OG, Verhaar MC, Chen Y, Vader P, Gremmels H, Posthuma G, et al. Cellular stress conditions are reflected in the protein and RNA content of endothelial cell-derived exosomes. J Extracell Vesicles 2012:1.
[24] Kumar A, Deep G. Hypoxia in tumor microenvironment regulates exosome biogenesis: molecular mechanisms and translational opportunities. Cancer Lett 2020(479):23–30.
[25] Chistiakov DA, Orekhov AN, Bobryshev YV. Cardiac extracellular vesicles in normal and infarcted heart. Int J Mol Sci 2016;17(1).
[26] Panigrahi GK, Deep G. Exosomes-based biomarker discovery for diagnosis and prognosis of prostate cancer. Front Biosci (Landmark Ed) 2017;22:1682–96.
[27] Kalluri R. The biology and function of exosomes in cancer. J Clin Invest 2016;126(4):1208–15.
[28] Asai H, Ikezu S, Tsunoda S, Medalla M, Luebke J, Haydar T, et al. Depletion of microglia and inhibition of exosome synthesis halt tau propagation. Nat Neurosci 2015;18(11):1584–93.
[29] Winston CN, Goetzl EJ, Akers JC, Carter BS, Rockenstein EM, Galasko D, et al. Prediction of conversion from mild cognitive impairment to dementia with neuronally derived blood exosome protein profile. Alzheimers Dement (Amst) 2016;3:63–72.
[30] Soria FN, Pampliega O, Bourdenx M, Meissner WG, Bezard E, Dehay B. Exosomes, an unmasked culprit in neurodegenerative diseases. Front Neurosci 2017;11:26.
[31] Fiandaca MS, Kapogiannis D, Mapstone M, Boxer A, Eitan E, Schwartz JB, et al. Identification of preclinical Alzheimer's disease by a profile of pathogenic proteins in neurally derived blood exosomes: a case-control study. Alzheimers Dement 2015;11(6) 600-7 e1.
[32] Kapogiannis D, Boxer A, Schwartz JB, Abner EL, Biragyn A, Masharani U, et al. Dysfunctionally phosphorylated type 1 insulin receptor substrate in neural-derived blood exosomes of preclinical Alzheimer's disease. FASEB J 2015;29(2):589–96.
[33] Vella LJ, Hill AF, Cheng L. Focus on extracellular vesicles: exosomes and their role in protein trafficking and biomarker potential in Alzheimer's and Parkinson's Disease. Int J Mol Sci 2016;17(2):173.
[34] Fiandaca MS, Kapogiannis D, Mapstone M, Boxer A, Eitan E, Schwartz JB, et al. Identification of preclinical Alzheimer's disease by a profile of pathogenic proteins in neurally derived blood exosomes: a case-control study. Alzheimers Dement 2015;11(6):600–7.
[35] Saeedi S, Israel S, Nagy C, Turecki G. The emerging role of exosomes in mental disorders. Transl Psychiatry 2019;9(1):122.
[36] Ebrahimkhani S, Vafaee F, Young PE, Hur SSJ, Hawke S, Devenney E, et al. Exosomal microRNA signatures in multiple sclerosis reflect disease status. Sci Rep 2017;7(1):14293.
[37] Shao H, Chung J, Lee K, Balaj L, Min C, Carter BS, et al. Chip-based analysis of exosomal mRNA mediating drug resistance in glioblastoma. Nat Commun 2015;6:6999.
[38] Yu S, Wei Y, Xu Y, Zhang Y, Li J, Zhang J. Extracellular vesicles in breast cancer drug resistance and their clinical application. Tumour Biol 2016;37(3):2849–61.
[39] Zhang H, Huang E, Kahwaji J, Nast CC, Li P, Mirocha J, et al. Plasma exosomes from HLA-sensitized kidney transplant recipients contain mRNA transcripts which predict development of antibody-mediated rejection. Transplantation 2017;101(10):2419–28.
[40] Kasner M, Gast M, Galuszka O, Stroux A, Rutschow S, Wang X, et al. Circulating exosomal microRNAs predict functional recovery after MitraClip repair of severe mitral regurgitation. Int J Cardiol 2016;215:402–5.
[41] Fan Z, Zhang Q, Chen H, He P, Li Y, Si M, et al. Circulating microRNAs as a biomarker to predict therapy efficacy in hepatitis C patients with different genotypes. Microb Pathog 2017;112:320–6.
[42] Rao PSS, O'Connell K, Finnerty TK. Potential role of extracellular vesicles in the pathophysiology of drug addiction. Mol Neurobiol 2018;55(8):6906–13.
[43] Hu G, Yao H, Chaudhuri AD, Duan M, Yelamanchili SV, Wen H, et al. Exosome-mediated shuttling of microRNA-29 regulates HIV Tat and morphine-mediated neuronal dysfunction. Cell Death Dis 2012;3:e381.
[44] Dominy SS, Brown JN, Ryder MI, Gritsenko M, Jacobs JM, Smith RD. Proteomic analysis of saliva in HIV-positive heroin addicts reveals proteins correlated with cognition. PLoS ONE 2014;9(4):e89366.
[45] Li H, Li C, Zhou Y, Luo C, Ou J, Li J, et al. Expression of microRNAs in the serum exosomes of methamphetamine-dependent rats vs. ketamine-dependent rats. Exp Ther Med 2018;15(4):3369–75.

[46] Saha B, Momen-Heravi F, Kodys K, Szabo G. MicroRNA cargo of extracellular vesicles from alcohol-exposed monocytes signals naive monocytes to differentiate into M2 macrophages. J Biol Chem 2016;291(1):149–59.
[47] Momen-Heravi F, Saha B, Kodys K, Catalano D, Satishchandran A, Szabo G. Increased number of circulating exosomes and their microRNA cargos are potential novel biomarkers in alcoholic hepatitis. J Transl Med 2015;13:261.
[48] Momen-Heravi F, Bala S, Kodys K, Szabo G. Exosomes derived from alcohol-treated hepatocytes horizontally transfer liver specific miRNA-122 and sensitize monocytes to. LPS. Sci Rep. 2015;5:9991.
[49] Hu G, Liao K, Niu F, Yang L, Dallon BW, Callen S, et al. Astrocyte EV-Induced lincRNA-Cox2 regulates microglial phagocytosis: implications for morphine-mediated neurodegeneration. Mol Ther Nucleic Acids 2018;13:450–63.
[50] Duan L, Ramachandran A, Akakpo JY, Weemhoff JL, Curry SC, Jaeschke H. Role of extracellular vesicles in release of protein adducts after acetaminophen-induced liver injury in mice and humans. Toxicol Lett 2019;301:125–32.
[51] Kumar S, El-Hage N, Batrakova E. Extracellular vesicles in HIV, drug abuse, and drug delivery. J Neuroimmune Pharmacol 2020;15(3):387–9.
[52] Shahjin F, Guda RS, Schaal VL, Odegaard K, Clark A, Gowen A, et al. Brain-derived extracellular vesicle microRNA signatures associated with in utero and. Postnatal Oxycodone Exposure. Cells. 2019;9(1).
[53] Kodidela S, Wang Y, Patters BJ, Gong Y, Sinha N, Ranjit S, et al. Proteomic profiling of exosomes derived from plasma of HIV-infected alcohol drinkers and cigarette smokers. J Neuroimmune Pharmacol 2020;15(3):501–19.
[54] Verma VK, Li H, Wang R, Hirsova P, Mushref M, Liu Y, et al. Alcohol stimulates macrophage activation through caspase-dependent hepatocyte derived release of CD40L containing extracellular vesicles. J Hepatol 2016;64(3):651–60.
[55] Toyama K, Kiyosawa N, Watanabe K, Ishizuka H. Identification of circulating miRNAs differentially regulated by opioid treatment. Int J Mol Sci 2017;18(9).
[56] Gould RW, Czoty PW, Porrino LJ, Nader MA. Social status in monkeys: effects of social confrontation on brain function and cocaine self-administration. Neuropsychopharmacology 2017;42(5):1093–102.
[57] Patterson SA, Deep G, Brinkley TE. Detection of the receptor for advanced glycation endproducts in neuronally-derived exosomes in plasma. Biochem Biophys Res Commun 2018;500(4):892–6.
[58] Pavelka N, Pelizzola M, Vizzardelli C, Capozzoli M, Splendiani A, Granucci F, et al. A power law global error model for the identification of differentially expressed genes in microarray data. BMC Bioinformat 2004;5:203.
[59] Kramer A, Green J, Pollard Jr. J, Tugendreich S. Causal analysis approaches in ingenuity pathway analysis. Bioinformatics 2014;30(4):523–30.
[60] Maldjian JA, Shively CA, Nader MA, Friedman DP, Whitlow CT. Multi-atlas library for eliminating normalization failures in non-human primates. Neuroinformatics 2016;14(2):183–90.
[61] Maldjian JA, Daunais JB, Friedman DP, Whitlow CT. Vervet MRI atlas and label map for fully automated morphometric analyses. Neuroinformatics 2014;12(4):543–50.
[62] Lehmann SM, Kruger C, Park B, Derkow K, Rosenberger K, Baumgart J, et al. An unconventional role for miRNA: let-7 activates Toll-like receptor 7 and causes neurodegeneration. Nat Neurosci 2012;15(6):827–35.
[63] Derkow K, Rossling R, Schipke C, Kruger C, Bauer J, Fahling M, et al. Distinct expression of the neurotoxic microRNA family let-7 in the cerebrospinal fluid of patients with Alzheimer's disease. PLoS ONE 2018;13(7):e0200602.
[64] Majer A, Medina SJ, Niu Y, Abrenica B, Manguiat KJ, Frost KL, et al. Early mechanisms of pathobiology are revealed by transcriptional temporal dynamics in hippocampal CA1 neurons of prion infected mice. PLoS Pathog 2012;8(11):e1003002.
[65] Cheng L, Doecke JD, Sharples RA, Villemagne VL, Fowler CJ, Rembach A, et al. Prognostic serum miRNA biomarkers associated with Alzheimer's disease shows concordance with neuropsychological and neuroimaging assessment. Mol Psychiatry 2015;20(10):1188–96.
[66] Watts ME, Williams SM, Nithianantharajah J, Claudianos C. Hypoxia-Induced MicroRNA-210 targets neurodegenerative pathways. Noncoding RNA 2018;4(2).
[67] Strang KH, Golde TE, Giasson BI. MAPT mutations, tauopathy, and mechanisms of neurodegeneration. Lab Invest 2019;99(7):912–28.
[68] Illan-Gala I, Pegueroles J, Montal V, Alcolea D, Vilaplana E, Bejanin A, et al. APP-derived peptides reflect neurodegeneration in frontotemporal dementia. Ann Clin Transl Neurol 2019;6(12):2518–30.
[69] Cheng N, Cai H, Belluscio L. In vivo olfactory model of APP-induced neurodegeneration reveals a reversible cell-autonomous function. J Neurosci 2011;31(39):13699–704.
[70] Giau VV, Bagyinszky E, Yang YS, Youn YC, An SSA, Kim SY. Genetic analyses of early-onset Alzheimer's disease using next generation sequencing. Sci Rep 2019;9(1):8368.
[71] McPherson CS, Lawrence AJ. The nuclear transcription factor CREB: involvement in addiction, deletion models and looking forward. Curr Neuropharmacol 2007;5(3):202–12.
[72] Sun WL, Quizon PM, Zhu J. Molecular mechanism: ERK signaling, drug addiction, and behavioral effects. Prog Mol Biol Transl Sci 2016;137:1–40.
[73] Ayatollahi-Mousavi SA, Asadikaram G, Nakhaee N, Izadi A, Keikha N. The effects of opium addiction on the immune system function in patients with fungal infection. Addict Health 2016;8(4):218–26.
[74] Rohrer JD, Woollacott IO, Dick KM, Brotherhood E, Gordon E, Fellows A, et al. Serum neurofilament light chain protein is a measure of disease intensity in frontotemporal dementia. Neurology 2016;87(13):1329–36.
[75] Rajapandi T, Greene LE, Eisenberg E. The molecular chaperones Hsp90 and Hsc70 are both necessary and sufficient to activate hormone binding by glucocorticoid receptor. J Biol Chem 2000;275(29):22597–604.
[76] Tertil M, Skupio U, Barut J, Dubovyk V, Wawrzczak-Bargiela A, Soltys Z, et al. Glucocorticoid receptor signaling in astrocytes is required for aversive memory formation. Transl Psychiatry 2018;8(1):255.
[77] White AJ, Wijeyekoon RS, Scott KM, Gunawardana NP, Hayat S, Solim IH, et al. The peripheral inflammatory response to Alpha-Synuclein and Endotoxin in Parkinson's Disease. Front Neurol 2018;9:946.
[78] Lema Tome CM, Tyson T, Rey NL, Grathwohl S, Britschgi M, Brundin P. Inflammation and alpha-synuclein's prion-like behavior in Parkinson's disease–is there a link? Mol Neurobiol 2013;47(2):561–74.
[79] von Boyen GB, Steinkamp M, Reinshagen M, Schafer KH, Adler G, Kirsch J. Proinflammatory cytokines increase glial fibrillary acidic protein expression in enteric glia. Gut 2004;53(2):222–8.
[80] Yang YF, Zhou YD, Hu JC, Luo FL, Xie Y, Shen YY, et al. Ficolin-A/2, acting as a new regulator of macrophage polarization, mediates the inflammatory response in experimental mouse colitis. Immunology 2017;151(4):433–50.
[81] Lopez-Dee Z, Pidcock K, Gutierrez LS. Thrombospondin-1: multiple paths to inflammation. Mediators Inflamm 2011;2011:296069.
[82] Liu G, Cooley MA, Jarnicki AG, Hsu AC, Nair PM, Haw TJ, et al. Fibulin-1 regulates the pathogenesis of tissue remodeling in respiratory diseases. JCI Insight 2016;1(9).
[83] Wang S, Song R, Wang Z, Jing Z, Wang S, Ma J. S100A8/A9 in Inflammation. Front Immunol 2018;9:1298.
[84] Piktel E, Levental I, Durnas B, Janmey PA, Bucki R. Plasma Gelsolin: indicator of inflammation and its potential as a diagnostic tool and therapeutic target. Int J Mol Sci 2018;19(9).
[85] Shamsuzzama Kumar L, Nazir A. Modulation of Alpha-synuclein expression and associated effects by MicroRNA Let-7 in Transgenic C. elegans. Front Mol Neurosci 2017;10:328.
[86] Asikainen S, Rudgalvyte M, Heikkinen L, Louhiranta K, Lakso M, Wong G, et al. Global microRNA expression profiling of Caenorhabditis elegans Parkinson's disease models. J Mol Neurosci 2010;41(1):210–8.
[87] Zhang N, Li WW, Lv CM, Gao YW, Liu XL, Zhao L. miR-16-5p and miR-19b-3p prevent amyloid beta-induced injury by targeting BACE1 in SH-SY5Y cells. Neuroreport 2020;31(3):205–12.
[88] Burgos K, Malenica I, Metpally R, Courtright A, Rakela B, Beach T, et al. Profiles of extracellular miRNA in cerebrospinal fluid and serum from patients with Alzheimer's and Parkinson's diseases correlate with disease status and features of pathology. PLoS ONE 2014;9(5):e94839.
[89] Ke S, Yang Z, Yang F, Wang X, Tan J, Liao B. Long Noncoding RNA NEAT1 Aggravates Abeta-Induced Neuronal Damage by Targeting miR-107 in Alzheimer's Disease. Yonsei Med J 2019;60(7):640–50.
[90] Sun L, Zhang T, Xiu W, Cao W, He M, Sun W, et al. MiR-107 overexpression attenuates neurotoxicity induced by 6-hydroxydopamine both in vitro and in vivo. Chem Biol Interact 2020;315:108908.
[91] Wang J, Chen C, Zhang Y. An investigation of microRNA-103 and microRNA-107 as potential blood-based biomarkers for disease risk and progression of Alzheimer's disease. J Clin Lab Anal 2020;34(1):e23006.